
000 SEMI-SUPERVISED LEARNING FOR MOLECULAR 001 002 GRAPHS VIA ENSEMBLE CONSENSUS 003 004

005 **Anonymous authors**

006 Paper under double-blind review

007 008 ABSTRACT 009

010 Machine learning is transforming molecular sciences by accelerating property
011 prediction, simulation, and the discovery of new molecules and materials. Acquir-
012 ing labeled data in these domains is often costly and time-consuming, whereas
013 large collections of unlabeled molecular data are readily available. Standard semi-
014 supervised learning methods often rely on label-preserving augmentations, which
015 are challenging to design in the molecular domain, where minor changes can drasti-
016 cally alter properties. In this work, we show that semi-supervised methods that rely
017 on an ensemble consensus can boost predictive accuracy across a diverse range of
018 molecular datasets, task types, and graph neural network architectures. Notably,
019 we show that training with an ensemble consensus objective results in an effect
020 similar to knowledge distillation; an individual member of an ensemble trained this
021 way often outperforms a full ensemble trained in a traditional supervised fashion.
022 In addition, this type of semi-supervised training reduces calibration error and is
023 robust over different datasets.

024 025 1 INTRODUCTION

026 In recent years, machine learning has emerged as a transformative tool in the molecular sciences,
027 accelerating discovery in areas ranging from predicting quantum mechanical properties (Schütt
028 et al., 2021; 2017; Musaelian et al., 2023; Wood et al., 2025) to discovering novel drugs (Wong
029 et al., 2024; Kellenberger et al., 2007; Vidler et al., 2013; Zhuang et al., 2014; Ren et al., 2023) and
030 catalysts (Pillai et al., 2023; Sun et al., 2024; Bai et al., 2025). However, despite recent efforts to
031 curate large labeled datasets (Merchant et al., 2023; Levine et al., 2025), the scarcity of labeled data
032 remains a fundamental bottleneck.

033 In materials and drug discovery, labels often come from computationally expensive simulations, such
034 as density functional theory (DFT), or resource-intensive laboratory measurements. Consequently,
035 datasets with specialized high-quality labels are typically small, while large databases of unlabeled
036 molecules (e.g., ZINC (Irwin et al., 2012; Kim et al., 2024)) are not fully exploited. This scenario—
037 abundant unlabeled data coupled with scarce labeled data—is an ideal setting for semi-supervised
038 learning (SSL).

039 Yet, many state-of-the-art methods are poorly suited for the molecular domain. Dominant techniques
040 such as consistency training (Berthelot et al., 2019; Sohn et al., 2020) critically depend on data
041 augmentation strategies that create perturbed copies of an input while preserving its label. Such
042 augmentations are notoriously difficult to design for molecules, where minor structural changes can
043 drastically alter the chemical properties we aim to predict. Meanwhile, approaches such as iterative
044 pseudo-labeling (Scudder, 1965; Riloff & Wiebe, 2003; Huang et al., 2022) hinges on the ability to
045 reliably rank predictions by confidence in order to select the best candidates for pseudo-labeling and
046 to avoid reinforcing model errors. This highlights a critical gap where standard SSL benchmarks and
047 algorithms do not translate well to the practical challenges of molecular science.

048 In this work, we build upon a class of SSL methods that does not require the explicit design of
049 data augmentations, but rather relies on an *ensemble consistency loss*. Specifically, we train a
050 model ensemble where each member learns from labeled data using a standard supervised loss and
051 from unlabeled data using a loss that promotes agreement among the ensemble members. While
052 ensemble coupling in self-supervised learning has been explored in previous work (Sajjadi et al., 2016;
053 Tarvainen & Valpola, 2018; Platanios, 2018), our formulation is theoretically grounded in an ensemble

loss ambiguity decomposition, trains in a single run, and exhibits a knowledge distillation-like effect that has not previously been discussed. As such, our work makes four core contributions:

1. We provide a theoretical motivation for our specific ensemble-consensus approach based on the formal decomposition of ensemble error, which justifies the consensus as a high-quality, better-than-average supervisory signal.
2. We demonstrate that our method robustly improves predictive accuracy across a wide range of molecular datasets and architectures for both regression and classification.
3. We show a powerful knowledge distillation-like effect, where a single model from our consensus-trained ensemble in almost all cases outperforms an entire ensemble trained in a traditional supervised fashion.
4. We also show that our approach, in comparison to other SSL methods reduces the calibration error and does not harm the prediction accuracy on the unlabeled training data.

2 BACKGROUND

Semi-Supervised Learning Semi-supervised learning (SSL) is a machine learning paradigm designed for settings with a small amount of labeled data and a much larger amount of unlabeled data. The idea is to leverage the unlabeled data to learn about the underlying structure of the data distribution $p(x)$, which in turn improves the model’s ability to learn the mapping from inputs to outputs, $p(y|x)$. Effective SSL methods are typically built upon one or more of the following assumptions:

- **Smoothness Assumption:** If two points x_1, x_2 are close in a high-density region of the underlying data manifold, their corresponding labels y_1, y_2 should also be close or identical.
- **Cluster Assumption:** The data tends to form distinct clusters, and points within the same cluster are likely to share the same label. This implies that a good decision boundary should lie in the low-density region between clusters.

Consistency Loss Consistency regularization is currently the most dominant family of SSL methods. The core idea is that the model’s prediction for an unlabeled data point should remain consistent under small perturbations. This directly enforces the smoothness assumption. A successful perturbation or data augmentation is one that explores the local neighborhood of a data point on the manifold without changing its label. The objective is typically formulated as minimizing a distance measure (e.g., Mean Squared Error or KL-Divergence) between the model’s predictions for two different augmentations of the same input:

$$\mathcal{L}_{\text{consistency}} = \mathbb{E}_{x_u \sim X_u} [D(f_\theta(\text{aug}_1(x_u)) || f_\theta(\text{aug}_2(x_u)))].$$

Different choices of the perturbations give rise to a wide range of methods. Π -models (Sajjadi et al., 2016) enforce that two predictions should be the same under transformations to the data, the use of dropout and random pooling for perturbations to the model. Each unlabeled datapoint is passed through the network twice and penalized for the difference in the predictions between the passes. The benefit of consistency loss is highly linked to the quality of the data augmentation techniques, as shown in (Xie et al., 2020). Temporal ensembling (Laine & Aila, 2017) builds upon this by maintaining an exponential moving average of predictions for each unlabeled example to create a more stable consistency target. Instead of applying a temporal averaging over the predictions, the mean-teacher method (Tarvainen & Valpola, 2018) averages the model weights and uses the predictions of that model as the consistency target. In the above works, the predictions can be seen as coming from a sort of pseudo-ensemble. As the members of this pseudo-ensemble are based on the trajectory or perturbation of a single network, the diversity of the predictions is reduced and biased, which reduces the prediction accuracy as we later highlight.

This problem can be mitigated by introducing multiple different initial weightings of the same architecture and training them in parallel to use as consistency targets. Chen et al. (2021) (cross pseudo supervision) proposes to do this for pixel-wise segmentation, where the prediction of each of the two ensemble members is hard labeled and used as the consistency target. Filipiak et al. (2022) further extends this for pixel-wise segmentation by using n ensemble models and taking all

108 combinations of hard labeled predictions as the consistency targets. Another paper that explores
109 different ensemble predictions is Platanios (2018). Here the ensemble members are restarted multiple
110 times during training, and the consensus target is computed from a trainable majority vote or Restricted
111 Boltzmann Machine. All the above methods can be seen as stemming from a broad class of SSL
112 methods that rely on the prediction of an ensemble to guide the training of the individual models to
113 improve predictive accuracy.

114 In many applications, there exist few or no data augmentations that preserve the label of a data point.
115 Examples include molecules, where the chemical properties can be changed significantly under small
116 changes to the molecule. This restricts the consistency loss methods to only rely on perturbations to
117 the model and not the data. This makes the class of ensemble-based SSL methods well-suited for the
118 problem.

119
120 **Pseudo-labeling** Pseudo-labeling (Yarowsky, 1995; Scudder, 1965; Riloff & Wiebe, 2003), also
121 known as self-training or entropy minimization, is a process where an initial model is trained on
122 the labeled data points and then used to predict labels for a large unlabeled dataset. The primary
123 risk of this method is confirmation bias: if the model generates an incorrect pseudo-label with high
124 confidence, it will reinforce its own mistake during retraining, leading to error propagation. To
125 mitigate this risk, modern SSL methods often integrate more sophisticated frameworks. For example,
126 one uncertainty-aware approach uses a model's evidential uncertainty to estimate the quality of
127 each pseudo-label. This enables an adaptive weighting scheme where high-uncertainty (low-quality)
128 pseudo-labels are given a smaller weight in the loss function, reducing their biasing effect. While this
129 can be effective, such a strategy requires an initial, full training phase on the labeled data before the
130 episodic pseudo-labeling can begin. It also introduces several additional tunable hyperparameters
131 related to its episodic schedule, which require careful tuning (Huang et al., 2022).
132

133 **Knowledge Distillation** Knowledge distillation (Buciluă et al., 2006; Hinton et al., 2015) was
134 proposed as a way of using a complex "teacher" model to transfer its knowledge to a simpler "student"
135 model. Usually, the teacher model is either a model with more parameters or the same model with
136 multiple predictions averaged over multiple augmentations of the input, but the use of an ensemble as
137 the teacher has also been explored (Hinton et al., 2015; Fukuda et al., 2017; Malinin et al., 2019). The
138 transfer of knowledge can be enforced at different levels, such as feature representations (Heo et al.,
139 2019) or intermediate layers (Zagoruyko & Komodakis, 2017). Approaches that match predictions
140 are most closely related to our work. Aligning student and teacher predictions resembles the use of
141 consistency targets in semi-supervised learning, with the key distinction that distillation is typically
142 applied post-hoc, and thus lacks a bootstrapping effect where the teacher also benefits from the
143 student's progress. Furthermore, knowledge distillation is often focused on preserving the uncertainty
144 calibration of the teacher or achieving computational efficiency by deploying the smaller student
145 model instead of the larger one.

146 3 THEORETICAL MOTIVATION

147 The theoretical motivation for our method is grounded in the formal relationship between an en-
148 semble's performance and that of its individual members. Ensemble performance is governed by
149 a fundamental trade-off between the accuracy of the individual models and the diversity of their
150 predictions. This relationship can be expressed through a loss decomposition, which shows that for
151 any convex loss function, the ensemble's loss is guaranteed to be less than or equal to the average of
152 the individual losses (Wood et al., 2024). This stems from Jensen's inequality and takes the general
153 form:

$$154 \text{Ensemble Loss} = \text{Average Individual Loss} - \text{Ambiguity} \quad (1)$$

155 The ambiguity (or diversity) term is a non-negative quantity measuring disagreement among the
156 members. This decomposition reveals that optimal ensemble performance requires not only accurate
157 individual models but also beneficial diversity.

158
159 **Mean Squared Error** This principle is most clearly illustrated in regression with Mean Squared
160 Error (MSE), where the decomposition is exact and well-established (Krogh & Vedelsby, 1994). For
161 an ensemble of M models $\{f_{\theta_m}\}_{m=1}^M$ with a mean prediction $\bar{f}(x)$, the decomposition is:

162
163
164
165
166

$$\underbrace{(y - \bar{f}(x))^2}_{\text{Ensemble MSE}} = \underbrace{\frac{1}{M} \sum_{m=1}^M (y - f_m(x))^2}_{\text{Average Individual MSE}} - \underbrace{\frac{1}{M} \sum_{m=1}^M (\bar{f}(x) - f_m(x))^2}_{\text{Ambiguity (Prediction Variance)}}. \quad (2)$$

167 Here, the ambiguity is simply the variance of the predictions around the ensemble mean, providing a
168 clear, label-independent measure of diversity.
169

170 **Cross-Entropy** The same principle extends to classification, though the decomposition for Cross-
171 Entropy (CE) loss is more nuanced. Using the geometric mean to average probabilities across the
172 ensemble yields a clean, label-independent decomposition, as in regression (Wood et al., 2024). An
173 exact decomposition is also available for the arithmetic mean:

174
175
176
177

$$\underbrace{-\mathbf{y} \cdot \ln \bar{\mathbf{f}}}_{\text{Ensemble CE Loss}} = -\underbrace{\frac{1}{M} \sum_{m=1}^M \mathbf{y} \cdot \ln \mathbf{f}_m}_{\text{Avg. Individual CE Loss}} - \underbrace{\sum_{c=1}^C y_c \ln \frac{\frac{1}{M} \sum_{m=1}^M f_{m,c}}{\left(\prod_{m=1}^M f_{m,c}\right)^{1/M}}}_{\text{Ambiguity (Label-Dependent)}}, \quad (3)$$

178 although here the ambiguity term is explicitly a function of the true label vector \mathbf{y} (where y_c is the
179 true probability of class c), making it label-dependent (Wood et al., 2024). Crucially, this ambiguity
180 term is still guaranteed to be non-negative, ensuring that the ensemble loss is always less than or
181 equal to the average individual loss.

182 Because the ensemble consensus is provably superior to the average individual model, using it as a
183 consistency target for unlabeled data is both effective and theoretically well-justified. In addition,
184 the ensemble prediction will be a useful signal as long as the models are better than random. This
185 suggests the ensemble prediction does not need to incorporate a warm-startup to provide a useful
186 predictive signal, as other works have observed (Tartavainen & Valpola, 2018) and used (Filipiak et al.,
187 2022; Platanios, 2018).

188
189

4 METHOD

190
191

4.1 FORMAL DESCRIPTION

193 We address a standard semi-supervised learning problem with a small set of labeled data, $\mathcal{D}_L =$
194 $\{(x_i, y_i)\}_{i=1}^{N_L}$, and a large set of unlabeled data, $\mathcal{D}_U = \{u_j\}_{j=1}^{N_U}$. We assume that both datasets are
195 drawn from the same underlying distribution. Our method utilizes a deep ensemble of M models,
196 $\bar{f} = \{f_{\theta_m}\}_{m=1}^M$, initialized with different random weights.

197 The training objective is defined on each model f_{θ_m} within the ensemble. At each training step, its
198 parameters θ_m are updated to minimize a composite loss, \mathcal{L}_m , which combines a standard supervised
199 signal \mathcal{L}_{sup} with an ensemble-driven consistency signal $\mathcal{L}_{\text{consistency}}$:

200
201

$$\mathcal{L}_m = \mathcal{L}_{\text{sup}}(f_{\theta_m}, B_L) + \gamma \mathcal{L}_{\text{consistency}}(f_{\theta_m}, \bar{f}, B_U), \quad (4)$$

202 where B_L and B_U are mini-batches of labeled and unlabeled data, respectively, and γ is the coupling
203 weight. During training, all models are updated simultaneously by minimizing the sum of their
204 individual losses i.e. $\mathcal{L} = \sum_{m=1}^M \mathcal{L}_m$. The first term, \mathcal{L}_{sup} , is the standard task-specific loss for model
205 f_{θ_m} on the labeled batch, such as mean squared error (MSE) for regression or cross-entropy (CE)
206 for classification. The second term, $\mathcal{L}_{\text{consistency}}$, provides the semi-supervised signal. It is calculated
207 for the model f_{θ_m} but depends on the outputs of the entire ensemble. For each unlabeled sample
208 $u \in B_U$, a consensus prediction, $\bar{f}(u)$, is computed by averaging the predictions of all M models:

209
210
211

$$\bar{f}(u) = \frac{1}{M} \sum_{m=1}^M f_{\theta_m}(u). \quad (5)$$

212 The Consensus prediction serves as the augmentation-free consistency target for model f_{θ_m} . We
213 penalize the discrepancy between model prediction and the ensemble consensus as
214

215

$$\mathcal{L}_{\text{consistency}}(f_{\theta_m}, \bar{f}, B_U) = \frac{1}{|B_U|} \sum_{u \in B_U} D(f_{\theta_m}(u), \bar{f}(u)). \quad (6)$$

216 Here, D is a suitable distance metric, for example, the task-specific supervised loss (e.g., L2 or
217 KL-divergence). In practice, when minimizing the loss we detach the gradient through $f(u)$, as the
218 consensus prediction is at least as accurate as the individual members' predictions on average (see
219 Appendix 3), ensuring that the ensemble is not encouraged to match the less accurate individual
220 predictions. Note, detaching the gradient has been observed to result in failure cases such as *learner*
221 *collusion* (Jeffares et al., 2023), but in our experience it does not appear to affect results negatively.
222

223 4.2 CONSENSUS–DIVERSITY DYNAMICS

224

225 Our proposed SSL training scheme directly manipulates the trade-off between accurate individual
226 models and high diversity among them. The unsupervised loss term, $\mathcal{L}_u(x_u) = \mathcal{L}(f_{\theta_i}(x_u), f_e(x_u))$,
227 creates a pull towards consensus by guiding each model f_{θ_i} to agree with the more stable ensemble
228 prediction f_e . This directly reduces the average individual error by providing a high-quality
229 supervisory signal for unlabeled data.

230 Simultaneously, this pull is counteracted by forces that preserve diversity. Each model begins from
231 a unique random initialization and follows a distinct optimization path due to the stochastic nature
232 of mini-batch SGD. This dynamic allows the models to converge to different solutions in parameter
233 space while still agreeing in function space.

234 Therefore, our method does not eliminate diversity but rather regulates it. The hyperparameter γ in
235 the total loss $\mathcal{L} = \mathcal{L}_l + \gamma \mathcal{L}_u$ serves as a direct control over this balance, allowing us to leverage the
236 unlabeled data to improve individual model accuracy without forcing a complete collapse in diversity.
237

238 Another benefit of this continuous learning between models is that we should be less likely get stuck
239 on early bad predictions, as can be the case with many forms of pseudo-labeling. This is because the
240 ensemble targets are "moving" with the ensemble. This can explain why we do not need to warmup
241 the coupling loss.
242

243 5 EXPERIMENTAL SETUP

244

245 We evaluate our method in two settings: First, on a quantum chemistry benchmark to demonstrate its
246 relevance for 3D-geometry-based molecular property prediction, and then across a diverse suite of
247 graph-level tasks to assess its broader applicability. All ensemble members were trained on identical
248 mini-batches of supervised data to simplify implementation. While this strategy reduces ensemble
249 diversity, potentially limiting the ensemble's predictive power, it allows for a fair direct comparison
250 with single models.
251

252 **Semi-supervised Protocol** To simulate the common scenario of data scarcity, we restrict the
253 supervised portion of our training to a small fraction for each task (10%). The remaining training
254 data (90%) is treated as unlabeled and is used exclusively for our ensemble consistency loss. Our
255 primary baseline is a standard deep ensemble of the same architecture, trained only on this small
256 labeled data subset. This setup allows us to directly measure the performance gain from leveraging
257 unlabeled data.
258

259 **Datasets** We test our method on a wide range of different datasets. We perform a prediction of
260 molecular properties in the QM9 dataset (Wu et al., 2018) for the main 12 targets, using the PaiNN
261 architecture Schütt et al. (2021) and an ensemble of size $M = 4$. To investigate how our method
262 scales, we study and compare performance on a single target (internal energy at 0K) for different
263 ensemble sizes ($M \in \{1, 2, 3, 4\}$). For broader validation of our method, we adopt a comprehensive
264 benchmark suite of graph-level tasks. We use three different graph-based architectures: GCN (Kipf &
265 Welling, 2017), GIN (Xu et al., 2019), and GatedGCN (Bresson & Laurent, 2018), adapting the code
266 from Luo et al. (2025) and following the testing procedure from Rampášek et al. (2023). We refer to
267 this suite of benchmarks as GNN+ benchmarks. The ensemble size is fixed to $M = 4$. To demonstrate
268 the general applicability of our method beyond the molecular domain, we perform experiments on
269 a benchmark of non-molecular graph datasets (see Appendix A.3). Further experiments showing
broader applicability beyond graphs are included in Appendix A.1. All datasets were split into 80%
training data, 10% validation data and 10% test data. While 10% of the training data is used as

270

271 Table 1: PaiNN performance (MAE) on QM9 targets. Results are reported as mean ± 1.96 standard
272 error of the mean over 3 seeds.

273	Target	Unit	Individual Member		Ensemble (M=4)		Mean-teacher
			Supervised	Supervised + SSL	Supervised	Supervised + SSL	
275	μ	D	.0740 \pm .0009	.0619 \pm .0004	.0683 \pm .0005	.0613 \pm .0004	.0721 \pm .0024
276	α	a_0^3	.1626 \pm .0006	.1327 \pm .0002	.1423 \pm .0005	.1307 \pm .0002	.1570 \pm .0020
277	ϵ_{HOMO}	meV	80.4961 \pm .5696	74.3067 \pm .2874	76.3702 \pm .4998	73.4216 \pm .2602	80.6 \pm .20
278	ϵ_{LUMO}	meV	62.0410 \pm .6873	57.7005 \pm .3890	59.3295 \pm .7226	57.2248 \pm .3748	62.0 \pm .8
279	$\Delta\epsilon$	meV	125.1425 \pm .7803	116.8389 \pm .7476	119.2652 \pm .6489	115.5238 \pm .7658	125.0 \pm .26
280	$\langle R^2 \rangle$	a_0^2	.8141 \pm .0194	.6189 \pm .0321	.6405 \pm .0133	.5696 \pm .0320	.799 \pm .040
281	ZPVE	meV	2.2163 \pm .0031	2.0117 \pm .0072	2.0714 \pm .0036	1.9884 \pm .0077	2.18 \pm .04
282	U_0	meV	24.8996 \pm .2355	19.9535 \pm .1812	20.8927 \pm .2374	19.3611 \pm .1819	24.7 \pm .85
283	U	meV	25.1262 \pm .3544	20.1439 \pm .1736	21.0568 \pm .3108	19.5466 \pm .1586	25.0 \pm .100
284	H	meV	25.1391 \pm .3319	20.1217 \pm .1890	21.0790 \pm .3171	19.5235 \pm .1905	24.8 \pm .96
285	G	meV	25.3738 \pm .3001	20.2668 \pm .2044	21.3625 \pm .2596	19.6880 \pm .1955	25.2 \pm .75
286	C_v	$\frac{\text{cal}}{\text{mol K}}$.0569 \pm .0005	.0450 \pm .0003	.0491 \pm .0005	.0440 \pm .0004	.0557 \pm .0005

285

286

287 labeled training data, the labels for the remaining 90% are discarded and this data is used as unlabeled
288 (unsupervised) training data.

289

290 **Hyperparameter Tuning** To ensure well-tuned models for datasets, the training hyperparameters
291 (learning rate and weight decay) were optimized for each target and model based on the valida-
292 tion performance of a single model in the supervised setting on the reduced labeled data. These
293 hyperparameters were kept fixed across different SSL methods tested to ensure fair comparison.
294 The parameters associated with each specific SSL method (coupling weight, mean-teacher decay,
295 etc.) were optimized based on validation accuracy for each target on QM9, and selected for the
296 GNN+ datasets based on the best value of ZINC. Details about the tuning procedures and selected
297 hyperparameters can be found in Appendix B.
298

299

300 **Evaluation** We evaluate the predictive performance for a single model, a standard ensemble, an
301 ensemble using SSL via ensemble consensus (ours) and an individual member from the latter. All
302 results are reported as the mean along with 1.96 times the standard error of the mean across different
303 seeds.

304

305

306

6 RESULTS

307

308

6.1 MOLECULAR PROPERTY PREDICTION ON QM9

309

310 The performance of our method on the 12 regression targets of the QM9 dataset is presented in Table 1.
311 The results indicate that training with the ensemble consistency loss (“Supervised + SSL”) reduces the
312 MAE across all evaluated targets when compared to the supervised-only baseline. This is observed for
313 both the individual PaiNN models and the four-member ensembles. Furthermore, a single individual
314 model from the coupled ensemble consistently outperforms the traditional supervised ensemble on
315 all targets.

316

317 The results for molecular property prediction on QM9 for different ensemble sizes are shown in
318 Table 2. Our SSL method outperforms a traditional ensemble for all sizes tested. Additionally,
319 using an individual member from an ensemble trained using our proposed SSL method, we not only
320 outperform a standard single model but also perform at a similar level to an ensemble that has only
321 been trained on the supervised data. The results are consistent across all ensemble sizes. Performance
322 increases with more ensemble members.

323

324

6.2 GNN+ BENCHMARK

325

326

327 To assess the broader applicability of our method, we evaluate it on several molecule-related bench-
328 marks using three different GNN architectures. The results are summarized in Table 3, and are
329 consistent with the performance on QM9. Looking at a single model, the addition of the SSL task

324
 325 Table 2: PaiNN performance (MAE) on QM9 internal energy at 0K in eV (U_0) for different ensemble
 326 sizes averaged across 3 seeds, with mean ± 1.96 standard error of the mean.

327 328 329 330 331 332 333	Size (M)	Individual member		Ensemble	
		334 335 336 337 338 339 340 341 342 343 344 345 346 347 348 349 350 351 352 353 354 355	340 341 342 343 344 345 346 347 348 349 350 351 352 353 354 355	341 342 343 344 345 346 347 348 349 350 351 352 353 354 355	342 343 344 345 346 347 348 349 350 351 352 353 354 355
1	24.8996 \pm .2355	–	–	–	–
2	–	20.7268 \pm .3312	21.9658 \pm .6189	20.2639 \pm .3139	–
3	–	20.4214 \pm .2054	21.2858 \pm .3761	19.8955 \pm .1882	–
4	–	19.9535 \pm .1812	20.8927 \pm .2374	19.3611 \pm .1819	–

336 Table 3: Performance on molecule-related benchmarks using different GNN architectures averaged
 337 across 5 seeds.

338 339 340 341 342 343 344 345 346 347 348 349 350 351 352 353 354 355	Dataset	Training	Metric	GCN		GIN		GatedGCN	
				340 341 342 343 344 345 346 347 348 349 350 351 352 353 354 355	341 342 343 344 345 346 347 348 349 350 351 352 353 354 355	341 342 343 344 345 346 347 348 349 350 351 352 353 354 355	342 343 344 345 346 347 348 349 350 351 352 353 354 355	343 344 345 346 347 348 349 350 351 352 353 354 355	344 345 346 347 348 349 350 351 352 353 354 355
ZINC		MAE \downarrow	Supervised	.3163 \pm .0121	.2934 \pm .0094	.2765 \pm .0247	.2516 \pm .0136	.2920 \pm .0113	.2646 \pm .0235
			Consensus	.2406 \pm .0150	.2367 \pm .0148	.2519 \pm .0246	.2485 \pm .0232	.2717 \pm .0230	.2658 \pm .0177
			Pairwise	.2462 \pm .0108	.2390 \pm .0102	.2500 \pm .0083	.2462 \pm .0092	.2653 \pm .0158	.2597 \pm .0171
			Mean teacher	.2884 \pm .0128	–	.2791 \pm .0117	–	.2830 \pm .0159	–
Peptides-struct		MAE \downarrow	Supervised	.3047 \pm .0098	.2932 \pm .0084	.2966 \pm .0067	.2918 \pm .0058	.2994 \pm .0105	.2908 \pm .0101
			Consensus	.2868 \pm .0062	.2866 \pm .0061	.2944 \pm .0072	.2938 \pm .0068	.2854 \pm .0061	.2848 \pm .0068
			Pairwise	.2933 \pm .0031	.2892 \pm .0029	.2916 \pm .0030	.2901 \pm .0029	.2898 \pm .0042	.2870 \pm .0041
			Mean teacher	.2985 \pm .0029	–	.2948 \pm .0023	–	.2953 \pm .0034	–
Peptides-func		AP \uparrow	Supervised	.4931 \pm .0346	.5105 \pm .0342	.4566 \pm .0224	.4765 \pm .0327	.4289 \pm .0051	.4444 \pm .0200
			Consensus	.5070 \pm .0141	.5160 \pm .0141	.4756 \pm .0180	.4815 \pm .0179	.4509 \pm .0144	.4580 \pm .0062
			Pairwise	.5055 \pm .0151	.5163 \pm .0150	.4739 \pm .0110	.4811 \pm .0117	.4463 \pm .0067	.4548 \pm .0069
			Mean teacher	.4893 \pm .0169	–	.4611 \pm .0130	–	.4352 \pm .0058	–
ogbg-molhiv		AUROC \uparrow	Supervised	.7216 \pm .0193	.7357 \pm .0212	.7329 \pm .0166	.7346 \pm .0165	.7312 \pm .0081	.7341 \pm .0107
			Consensus	.7308 \pm .0218	.7357 \pm .0212	.7339 \pm .0149	.7347 \pm .0153	.7361 \pm .0069	.7383 \pm .0073
			Pairwise	.7247 \pm .0160	.7336 \pm .0146	.7273 \pm .0128	.7294 \pm .0128	.7375 \pm .0052	.7403 \pm .0050
			Mean teacher	.7213 \pm .0161	–	.6996 \pm .0207	–	.7295 \pm .0165	–
ogbg-molpcba		AP \uparrow	Supervised	.1368 \pm .0025	.1578 \pm .0030	.1421 \pm .0026	.1567 \pm .0029	.1615 \pm .0034	.1779 \pm .0043
			Consensus	.1476 \pm .0023	.1585 \pm .0026	.1496 \pm .0033	.1567 \pm .0039	.1701 \pm .0036	.1781 \pm .0034
			Pairwise	.1471 \pm .0027	.1597 \pm .0028	.1498 \pm .0021	.1574 \pm .0024	.1674 \pm .0032	.1765 \pm .0034
			Mean teacher	.1435 \pm .0016	–	.1479 \pm .0037	–	.1669 \pm .0028	–

356
 357
 358 consistently improves performance over the supervised-only baseline across all datasets and architectures.
 359 This performance gain also translates to the full ensembles, which show improvement when
 360 trained with the consistency loss. The performance of a single model trained with our SSL method
 361 often exceeds that of an entire ensemble trained only on labeled data.

7 DISCUSSION

362 Our experiments on QM9 and the more varied GNN+ benchmark show that our ensemble-based
 363 SSL framework consistently improves model performance in low-data regimes. The most significant
 364 finding is the substantial boost in accuracy for individual models, a direct result of the knowledge
 365 transferred from the ensemble’s consensus on unlabeled data. This finding is similar to the idea
 366 ensemble distilling (Hinton et al., 2015), where the knowledge of an ensemble is transferred to a
 367 single, smaller model, except that our method inherently produces knowledgeable single models.
 368 This is explained through the semi-supervised effect on the entire ensemble, resulting in even better
 369 ensemble consensus targets for individual models to learn from. This has a key practical benefit:
 370 while the method requires an ensemble during training, a single, improved model can be deployed for
 371 inference. This offers a valuable trade-off, where an increased one-time training cost yields a final
 372 model that is both highly accurate and computationally efficient at inference time. Chemical property
 373 screening is a compelling use case, as vast databases of molecules need to be screened resulting in a
 374 high inference cost, while the available labeled data and models are small making training cheap. It
 375 is noteworthy that for datasets where the parameter related to SSL (γ or the mean-teacher decay) was
 376

378 not directly tuned, the improvement in predictive accuracy was noticeably smaller. This indicates the
379 SSL parameter is highly dependent on the specific dataset.
380

381 As shown in Table 2, the predictive performance scales with the number of members in the coupled
382 ensemble. Individual models from the ensemble trained with our method consistently perform at
383 a similar level to an entire traditional ensemble across all ensemble sizes. This finding is further
384 supported in Appendix A.1.

385 **Limitations** The primary limitation of our approach is the computational overhead associated with
386 training an ensemble consensus model. Transfer learning is another method that is often used in
387 sparsely-labeled settings, which we have not compared against.
388

389 **Future work** Our findings suggest several promising avenues for future research. While this work
390 created a semi-supervised split from a fully labeled dataset, a compelling next step would be to
391 use all available labeled data for supervision while introducing a separate, truly unlabeled dataset.
392 This would more directly quantify the benefit of leveraging vast, external chemical libraries and
393 be of interest in a practical setting. Using ensembles for semi-supervised learning also opens the
394 direction for improving accuracy in a principled manner by diversifying the ensemble members
395 through existing techniques. Furthermore, different strategies for how to couple our ensemble can be
396 investigated. While first experiments (Appendix D.4) suggest that a constant coupling weight and an
397 inclusion of the ensemble consistency loss throughout the whole training yield the best results, these
398 findings still need to be validated through further experimentation on a broader range of datasets to
399 find the optimal strategy. Only including the unsupervised data in the later part during training could
400 potentially result in similar predictive performance, while reducing computational cost.
401

402 REFERENCES

403 Eric Arazo, Diego Ortego, Paul Albert, Noel E. O’Connor, and Kevin McGuinness. Pseudo-Labeling
404 and Confirmation Bias in Deep Semi-Supervised Learning. 6 2020.

405 Ruilin Bai, Yu Yao, Qiaosong Lin, Lize Wu, Zhen Li, Huijuan Wang, Mingze Ma, Di Mu,
406 Lingxiang Hu, Hai Yang, Weihan Li, Shaolong Zhu, Xiaojun Wu, Xianhong Rui, and Yan
407 Yu. Preferable single-atom catalysts enabled by natural language processing for high energy
408 density Na-S batteries. *Nature Communications*, 16(1):5827, 7 2025. ISSN 2041-1723. doi:
409 10.1038/s41467-025-60931-x.
410

411 David Berthelot, Nicholas Carlini, Ian Goodfellow, Nicolas Papernot, Avital Oliver, and Colin Raffel.
412 MixMatch: A Holistic Approach to Semi-Supervised Learning. 10 2019.

413 Xavier Bresson and Thomas Laurent. Residual Gated Graph ConvNets. 4 2018.

414 Cristian Buciluă, Rich Caruana, and Alexandru Niculescu-Mizil. Model compression. In *Proceedings
415 of the 12th ACM SIGKDD international conference on Knowledge discovery and data mining*, pp.
416 535–541, 2006.

417 Xiaokang Chen, Yuhui Yuan, Gang Zeng, and Jingdong Wang. Semi-Supervised Semantic Segmen-
418 tation with Cross Pseudo Supervision. 6 2021.

419 Dominik Filipiak, Piotr Tempczyk, and Marek Cygan. n-CPS: Generalising Cross Pseudo Supervision
420 to Networks for Semi-Supervised Semantic Segmentation. 4 2022.

421 Takashi Fukuda, Masayuki Suzuki, Gakuto Kurata, Samuel Thomas, Jia Cui, and Bhuvana Ram-
422 abhadran. Efficient knowledge distillation from an ensemble of teachers. In *Interspeech*, pp.
423 3697–3701, 2017.

424 Kaiming He, Xiangyu Zhang, Shaoqing Ren, and Jian Sun. Deep Residual Learning for Image
425 Recognition. 12 2015.

426 Byeongho Heo, Minsik Lee, Sangdoo Yun, and Jin Young Choi. Knowledge transfer via distillation
427 of activation boundaries formed by hidden neurons. *Proceedings of the AAAI Conference on
428 Artificial Intelligence*, 33(01):3779–3787, Jul. 2019. doi: 10.1609/aaai.v33i01.33013779. URL
429 <https://ojs.aaai.org/index.php/AAAI/article/view/4264>.

432 Geoffrey Hinton, Oriol Vinyals, and Jeff Dean. Distilling the knowledge in a neural network. *arXiv*
433 *preprint arXiv:1503.02531*, 2015.

434

435 Kexin Huang, Vishnu Sresht, Brajesh Rai, and Mykola Bordyuh. Uncertainty-aware pseudo-labeling
436 for quantum calculations. In James Cussens and Kun Zhang (eds.), *Proceedings of the Thirty-*
437 *Eighth Conference on Uncertainty in Artificial Intelligence*, volume 180 of *Proceedings of Machine*
438 *Learning Research*, pp. 853–862. PMLR, 01–05 Aug 2022. URL <https://proceedings.mlr.press/v180/huang22a.html>.

439

440 John J. Irwin, Teague Sterling, Michael M. Mysinger, Erin S. Bolstad, and Ryan G. Coleman. ZINC:
441 A Free Tool to Discover Chemistry for Biology. *Journal of Chemical Information and Modeling*,
442 52(7):1757–1768, 7 2012. ISSN 1549-9596. doi: 10.1021/ci3001277.

443

444 Alan Jeffares, Tennison Liu, Jonathan Crabbé, and Mihaela van der Schaar. Joint Training of Deep
445 Ensembles Fails Due to Learner Collusion. 10 2023.

446

447 Esther Kellenberger, Jean-Yves Springael, Marc Parmentier, Muriel Hachet-Haas, Jean-Luc Galzi,
448 and Didier Rognan. Identification of Nonpeptide CCR5 Receptor Agonists by Structure-based
449 Virtual Screening. *Journal of Medicinal Chemistry*, 50(6):1294–1303, 3 2007. ISSN 0022-2623.
450 doi: 10.1021/jm061389p.

451 Sunghwan Kim, Jie Chen, Tiejun Cheng, Asta Gindulyte, Jia He, Siqian He, Qingliang Li, Benjamin A
452 Shoemaker, Paul A Thiessen, Bo Yu, Leonid Zaslavsky, Jian Zhang, and Evan E Bolton. Pubchem
453 2025 update. *Nucleic Acids Research*, 53(D1):D1516–D1525, 11 2024. ISSN 1362-4962. doi:
454 10.1093/nar/gkae1059. URL <https://doi.org/10.1093/nar/gkae1059>.

455

456 Thomas N. Kipf and Max Welling. Semi-Supervised Classification with Graph Convolutional
457 Networks. 2 2017.

458

459 Anders Krogh and Jesper Vedelsby. Neural Network Ensembles, Cross Validation, and Active Learn-
460 ing. In G Tesauro, D Touretzky, and T Leen (eds.), *Advances in Neural Information Processing Sys-*
461 *tems*, volume 7. MIT Press, 1994. URL https://proceedings.neurips.cc/paper_files/paper/1994/file/b8c37e33defde51cf91e1e03e51657da-Paper.pdf.

462

463 Samuli Laine and Timo Aila. Temporal Ensembling for Semi-Supervised Learning. 3 2017.

464

465 Daniel S. Levine, Muhammed Shuaibi, Evan Walter Clark Spotte-Smith, Michael G. Taylor, Muham-
466 mad R. Hasyim, Kyle Michel, Ilyes Batatia, Gábor Csányi, Misko Dzamba, Peter Eastman,
467 Nathan C. Frey, Xiang Fu, Vahe Gharakhanyan, Aditi S. Krishnapriyan, Joshua A. Rackers, San-
468 jeev Raja, Ammar Rizvi, Andrew S. Rosen, Zachary Ulissi, Santiago Vargas, C. Lawrence Zitnick,
469 Samuel M. Blau, and Brandon M. Wood. The open molecules 2025 (omol25) dataset, evaluations,
470 and models, 2025. URL <https://arxiv.org/abs/2505.08762>.

471

472 Yuankai Luo, Lei Shi, and Xiao-Ming Wu. Can Classic GNNs Be Strong Baselines for Graph-level
473 Tasks? Simple Architectures Meet Excellence. 5 2025.

474

475 Andrey Malinin, Bruno Mlodzeniec, and Mark Gales. Ensemble distribution distillation. *arXiv*
476 *preprint arXiv:1905.00076*, 2019.

477

478 Amil Merchant, Simon Batzner, Samuel S. Schoenholz, Muratahan Aykol, Gowoon Cheon, and
479 Ekin Dogus Cubuk. Scaling deep learning for materials discovery. *Nature*, 2023. doi: 10.1038/s41586-023-06735-9.

480

481 Shambhavi Mishra, Balamurali Murugesan, Ismail Ben Ayed, Marco Pedersoli, and Jose Dolz. Do
482 not trust what you trust: Miscalibration in Semi-supervised Learning. 3 2024.

483

484 Albert Musaelian, Simon Batzner, Anders Johansson, Lixin Sun, Cameron J. Owen, Mordechai
485 Kornbluth, and Boris Kozinsky. Learning local equivariant representations for large-scale
atomistic dynamics. *Nature Communications*, 14(1):579, 2 2023. ISSN 2041-1723. doi:
10.1038/s41467-023-36329-y.

486 Hemanth Somarajan Pillai, Yi Li, Shih-Han Wang, Noushin Omidvar, Qingmin Mu, Luke E K
487 Achenie, Frank Abild-Pedersen, Juan Yang, Gang Wu, and Hongliang Xin. Interpretable design
488 of Ir-free trimetallic electrocatalysts for ammonia oxidation with graph neural networks. *Nature
489 Communications*, 14(1):792, 2023. ISSN 2041-1723. doi: 10.1038/s41467-023-36322-5. URL
490 <https://doi.org/10.1038/s41467-023-36322-5>.

491 Emmanouil Antonios Platanios. Agreement-based learning. 6 2018. URL <http://arxiv.org/abs/1806.01258>.

492

493 Ladislav Rampášek, Mikhail Galkin, Vijay Prakash Dwivedi, Anh Tuan Luu, Guy Wolf, and Do-
494 minique Beaini. Recipe for a General, Powerful, Scalable Graph Transformer. 1 2023.

495

496 Feng Ren, Xiao Ding, Min Zheng, Mikhail Korzinkin, Xin Cai, Wei Zhu, Alexey Mantsyzov, Alex
497 Aliper, Vladimir Aladinskiy, Zhongying Cao, Shanshan Kong, Xi Long, Bonnie Hei Man Liu,
498 Yingtao Liu, Vladimir Naumov, Anastasia Shneyderman, Ivan V. Ozerov, Ju Wang, Frank W. Pun,
499 Daniil A. Polykovskiy, Chong Sun, Michael Levitt, Alán Aspuru-Guzik, and Alex Zhavoronkov.
500 AlphaFold accelerates artificial intelligence powered drug discovery: efficient discovery of a novel
501 CDK20 small molecule inhibitor. *Chemical Science*, 14(6):1443–1452, 2023. ISSN 2041-6520.
502 doi: 10.1039/D2SC05709C.

503

504 Ellen Riloff and Janyce Wiebe. Learning extraction patterns for subjective expressions. In *Proceedings
505 of the 2003 Conference on Empirical Methods in Natural Language Processing*, pp. 105–112,
506 2003. URL <https://aclanthology.org/W03-1014/>.

507

508 Mehdi Sajjadi, Mehran Javanmardi, and Tolga Tasdizen. Regularization With Stochastic Transforma-
509 tions and Perturbations for Deep Semi-Supervised Learning. 6 2016.

510

511 Kristof T. Schütt, Pieter-Jan Kindermans, Huziel E. Sauceda, Stefan Chmiela, Alexandre Tkatchenko,
512 and Klaus-Robert Müller. SchNet: A continuous-filter convolutional neural network for modeling
513 quantum interactions. 12 2017.

514

515 Kristof T. Schütt, Oliver T. Unke, and Michael Gastegger. Equivariant message passing for the
516 prediction of tensorial properties and molecular spectra. 6 2021.

517

518 H. Scudder. Probability of error of some adaptive pattern-recognition machines. *IEEE Transactions
519 on Information Theory*, 11(3):363–371, 1965. doi: 10.1109/TIT.1965.1053799.

520

521 Kihyuk Sohn, David Berthelot, Chun-Liang Li, Zizhao Zhang, Nicholas Carlini, Ekin D. Cubuk,
522 Alex Kurakin, Han Zhang, and Colin Raffel. FixMatch: Simplifying Semi-Supervised Learning
523 with Consistency and Confidence. 11 2020.

524

525 Jikai Sun, Rui Tu, Yuchun Xu, Hongyan Yang, Tie Yu, Dong Zhai, Xiuqin Ci, and Weiqiao Deng.
526 Machine learning aided design of single-atom alloy catalysts for methane cracking. *Nature
527 Communications*, 15(1):6036, 7 2024. ISSN 2041-1723. doi: 10.1038/s41467-024-50417-7.

528

529 Antti Tarvainen and Harri Valpola. Mean teachers are better role models: Weight-averaged consistency
530 targets improve semi-supervised deep learning results. 4 2018.

531

532 Lewis R. Vidler, Panagis Filippakopoulos, Oleg Fedorov, Sarah Picaud, Sarah Martin, Michael
533 Tomsett, Hannah Woodward, Nathan Brown, Stefan Knapp, and Swen Hoelder. Discovery of
534 Novel Small-Molecule Inhibitors of BRD4 Using Structure-Based Virtual Screening. *Journal of
535 Medicinal Chemistry*, 56(20):8073–8088, 10 2013. ISSN 0022-2623. doi: 10.1021/jm4011302.

536

537 Felix Wong, Erica J. Zheng, Jacqueline A. Valeri, Nina M. Donghia, Melis N. Anahtar, Satotaka
538 Omori, Alicia Li, Andres Cubillos-Ruiz, Aarti Krishnan, Wengong Jin, Abigail L. Manson, Jens
539 Friedrichs, Ralf Helbig, Behnoush Hajian, Dawid K. Fiejtek, Florence F. Wagner, Holly H. Souter,
Ashlee M. Earl, Jonathan M. Stokes, Lars D. Renner, and James J. Collins. Discovery of a structural
class of antibiotics with explainable deep learning. *Nature*, 626(7997):177–185, 2 2024. ISSN
0028-0836. doi: 10.1038/s41586-023-06887-8.

540

541 Brandon M. Wood, Misko Dzamba, Xiang Fu, Meng Gao, Muhammed Shuaibi, Luis Barroso-Luque,
542 Kareem Abdelmaqsoud, Vahe Gharakhanyan, John R. Kitchin, Daniel S. Levine, Kyle Michel,
543 Anuroop Sriram, Taco Cohen, Abhishek Das, Ammar Rizvi, Sushree Jagriti Sahoo, Zachary W.
544 Ulissi, and C. Lawrence Zitnick. UMA: A Family of Universal Models for Atoms. 6 2025.

540 Danny Wood, Tingting Mu, Andrew Webb, Henry Reeve, Mikel Luján, and Gavin Brown. A
541 unified theory of diversity in ensemble learning, 2024. URL [https://arxiv.org/abs/](https://arxiv.org/abs/2301.03962)
542 2301.03962.

543 Zhenqin Wu, Bharath Ramsundar, Evan N. Feinberg, Joseph Gomes, Caleb Geniesse, Aneesh S.
544 Pappu, Karl Leswing, and Vijay Pande. MoleculeNet: A Benchmark for Molecular Machine
545 Learning. 10 2018.

546 Qizhe Xie, Zihang Dai, Eduard Hovy, Minh-Thang Luong, and Quoc V. Le. Unsupervised Data
547 Augmentation for Consistency Training. 11 2020.

548 Keyulu Xu, Weihua Hu, Jure Leskovec, and Stefanie Jegelka. How Powerful are Graph Neural
549 Networks? 2 2019.

550 David Yarowsky. Unsupervised word sense disambiguation rivaling supervised methods. In *33rd*
551 *Annual Meeting of the Association for Computational Linguistics*, pp. 189–196, Cambridge,
552 Massachusetts, USA, June 1995. Association for Computational Linguistics. doi: 10.3115/981658.
553 981684. URL <https://aclanthology.org/P95-1026/>.

554 Sergey Zagoruyko and Nikos Komodakis. Paying more attention to attention: Improving the
555 performance of convolutional neural networks via attention transfer, 2017. URL <https://arxiv.org/abs/1612.03928>.

556 Chunlin Zhuang, Sreekanth Narayananpillai, Wannian Zhang, Yuk Yin Sham, and Chengguo Xing.
557 Rapid Identification of Keap1–Nrf2 Small-Molecule Inhibitors through Structure-Based Virtual
558 Screening and Hit-Based Substructure Search. *Journal of Medicinal Chemistry*, 57(3):1121–1126,
559 2 2014. ISSN 0022-2623. doi: 10.1021/jm4017174.

560
561
562
563
564
565
566
567
568
569
570
571
572
573
574
575
576
577
578
579
580
581
582
583
584
585
586
587
588
589
590
591
592
593

SUPPLEMENTARY MATERIAL

A EXTENDED STUDIES

A.1 SCALING WITH NUMBER OF ENSEMBLE MEMBERS

We also investigate the predictive accuracy scaling with the number of ensemble members to larger than 4 sizes. Ensembles of these sizes were not feasible to do on any of the graph datasets, so we instead use the original computer vision version of CIFAR-10. This also validates that our method works for other domains than graphs. We use ResNet-18 (He et al., 2015) with 5,000 labeled and 40,000 unlabeled data-points without any data augmentations. We performed an exhaustive hyperparameter sweep using a single seed over learning rate (0.1, 0.075, 0.05, 0.025, 0.01, 0.0075, 0.005, 0.0025, 0.001), and weight decay (0.01, 0.025, 0.05, 0.075, 0.1, 0.25, 0.5) for the purely supervised model. The number of epochs and learning rate annealing was fixed at a number informally found to work. The parameters of best performing model on validation accuracy at the last epoch was selected. The optimal values can be found in 14. The coupling weight was fixed kept at $\gamma = 1$.

The hyper-parameters can be found in Appendix B.3. From the accuracy results in Table 4 and calibration scores in section A.2, we see a significant increase in accuracy and calibration scores going from a single model to a coupled ensemble with just two models. Interestingly, the individual prediction accuracy of a model trained in a coupled ensemble of two models outperforms the ensemble prediction from all decoupled ensemble sizes tested. This highlights the semi-supervised effect from using unlabeled data for training. Looking at the calibration metrics in Appendix A.2, we see that the calibration results for the coupled ensemble are worse than the uncoupled one. This is often seen in self-supervised learning, as the "self-validating" training can result in worse calibration from confirmation bias (Arazo et al., 2020; Mishra et al., 2024). Surprisingly, we see the individual calibration improving over the decoupled model (i.e., a single model), and also improving as the number of ensemble members increases.

Table 4: Predictive accuracy (%) on CIFAR-10 validation, comparing Decoupled and Coupled models. The values represent mean \pm 1.96 standard error of the mean.

Ensemble size	Individual Accuracy %		Ensemble Accuracy (%)	
	Decoupled	Coupled	Decoupled	Coupled
1	59.08 \pm 1.35
2	...	66.36 \pm 0.45	62.51 \pm 0.40	66.96 \pm 0.47
4	...	67.24 \pm 0.40	64.65 \pm 0.46	67.92 \pm 0.49
8	...	67.64 \pm 0.35	65.73 \pm 0.51	68.34 \pm 0.34
16	...	67.75 \pm 0.32	66.41 \pm 0.57	68.54 \pm 0.45
32	...	67.75 \pm 0.30	66.64 \pm 0.37	68.52 \pm 0.35

648 A.2 CALIBRATION METRICS ON CIFAR-10
649
650

651 Table 5: NLL on CIFAR-10, comparing decoupled and coupled models. The values represent mean
652 ± 1.96 standard error of the mean.
653

654
655
656
657
658
659
660
661
662
663
664
665
666
667
668
669
670
671
672
673
674
675
676
677
678
679
680
681
682
683
684
685
686
687
688
689
690
691
692
693
694
695
696
697
698
699
700
701

Ensemble size	NLL			
	Individual member		Ensemble	
	Decoupled	Coupled	Decoupled	Coupled
1	1.543 \pm 0.109
2	:	1.217 \pm 0.021	1.267 \pm 0.020	1.161 \pm 0.021
4	:	1.169 \pm 0.019	1.121 \pm 0.012	1.096 \pm 0.019
8	:	1.142 \pm 0.017	1.048 \pm 0.015	1.064 \pm 0.016
16	:	1.126 \pm 0.015	1.007 \pm 0.015	1.047 \pm 0.014
32	:	1.123 \pm 0.019	0.990 \pm 0.011	1.042 \pm 0.018

669 Table 6: AUC-ROC on CIFAR-10, comparing decoupled and coupled models. The values represent
670 mean ± 1.96 standard error of the mean.
671

672
673
674
675
676
677
678
679
680
681
682
683
684
685
686
687
688
689
690
691
692
693
694
695
696
697
698
699
700
701

Ensemble size	AUC-ROC			
	Individual member		Ensemble	
	Decoupled	Coupled	Decoupled	Coupled
1	.8885 \pm .0075
2	:	.9250 \pm .0020	.9125 \pm .0021	.9292 \pm .0020
4	:	.9295 \pm .0019	.9266 \pm .0016	.9349 \pm .0019
8	:	.9316 \pm .0019	.9336 \pm .0021	.9377 \pm .0018
16	:	.9323 \pm .0016	.9384 \pm .0019	.9386 \pm .0015
32	:	.9329 \pm .0019	.9409 \pm .0017	.9394 \pm .0019

687 Table 7: ECE on CIFAR-10, comparing decoupled and coupled models. The values represent mean
688 ± 1.96 standard error of the mean.
689

690
691
692
693
694
695
696
697
698
699
700
701

Ensemble size	ECE			
	Individual member		Ensemble	
	Decoupled	Coupled	Decoupled	Coupled
1	.2210 \pm .0357
2	:	.1713 \pm .0041	.1128 \pm .0057	.1512 \pm .0049
4	:	.1609 \pm .0034	.0591 \pm .0043	.1369 \pm .0040
8	:	.1548 \pm .0031	.0320 \pm .0043	.1301 \pm .0035
16	:	.1494 \pm .0028	.0243 \pm .0033	.1235 \pm .0030
32	:	.1485 \pm .0044	.0207 \pm .0043	.1226 \pm .0043

702
 703 Table 8: Brier score on CIFAR-10, comparing decoupled and coupled models. The values represent
 704 mean ± 1.96 standard error of the mean.

705 706 707 708 709 710 711 712 713 714 715 716 717	Ensemble size	Brier			
		Individual member		Ensemble	
		Decoupled	Coupled	Decoupled	Coupled
1		.4854 \pm .0271
2		⋮	.5594 \pm .0042	.4585 \pm .0041	.5530 \pm .0040
4		⋮	.5654 \pm .0040	.4422 \pm .0047	.5572 \pm .0040
8		⋮	.5676 \pm .0048	.4316 \pm .0050	.5588 \pm .0047
16		⋮	.5652 \pm .0044	.4283 \pm .0049	.5563 \pm .0043
32		⋮	.5649 \pm .0030	.4263 \pm .0033	.5558 \pm .0030

718
 719
 720
 721 A.3 NON-CHEMICAL GNN+ DATASETS
 722

724 Results for non-chemical GNN+ datasets are shown in Table 9. Note the consensus and mean-teacher
 725 run for the GatedGCN models were not computed, as the models were too large to fit in memory.
 726
 727
 728
 729

730 Table 9: Performance on non-molecule-related benchmarks, comparing supervised models with those
 731 using additional self-supervised learning (SSL). Results are shown for individual models (Individual)
 732 and the full ensemble (Ensemble). Results are the mean ± 1.96 standard error of the mean over 5
 733 different seeds.

734 735	Dataset	Training	Metric	GCN		GIN		GatedGCN	
				Individual	Ensemble	Individual	Ensemble	Individual	Ensemble
736 737 738	CIFAR-10	Supervised		50.44 \pm .33	55.38 \pm .49	50.46 \pm .34	53.90 \pm .50	57.69 \pm .34	61.23 \pm .45
		Consensus	Acc (%) \uparrow	55.33 \pm .31	57.11 \pm .42	54.30 \pm .36	55.60 \pm .31	-	-
		Mean teacher	Acc (%) \uparrow	50.64 \pm .28		50.99 \pm .86	-	-	-
739 740	MNIST	Supervised		96.61 \pm .07	96.97 \pm .04	96.26 \pm .10	96.73 \pm .13	96.96 \pm .05	97.38 \pm .11
		Consensus	Acc (%) \uparrow	96.82 \pm .08	96.93 \pm .11	96.68 \pm .09	96.82 \pm .11	97.48 \pm .06	97.57 \pm .07
		Mean teacher	Acc (%) \uparrow	96.55 \pm .06	-	96.31 \pm .11	-	96.84 \pm .13	-

741
 742
 743
 744 B HYPERPARAMETERS
 745

746 B.1 QM9
 747

748 Our hyperparameter search for QM9 followed a two-step process. First, we started with baseline
 749 hyperparameters from a fully supervised setting and tuned the learning rate and weight decay for a
 750 single model on the 10% labeled data subset. Second, using these optimized parameters, we then tuned
 751 the coupling weight (γ) for the size-4 ensemble by searching over $\{1.0, 0.1, 0.01, 0.001, 0.0001\}$. The
 752 coupling weight swept for the mean-teacher was $\{0.9, 0.95, 0.99, 0.995, 0.999\}$. Final a architectural
 753 and training configurations are detailed in Table 10 and Table 11.

756
757 Table 10: Hyperparameter Configuration for QM9. These are fixed across all targets.
758
759
760
761
762
763
764
765
766
767
768
769
770
771
772
773

Hyperparameter	Value
Training	
Batch size	32
Epochs	1000
Optimizer	AdamW
Scheduler	Cosine annealing
Coupling	
Unsupervised loss criterion	L2

774 Table 11: Additional hyperparameter Configuration for QM9 for different targets.
775

Target	Learning rate	Weight decay	Coupling weight	Mean teacher decay
μ	1e-3	1e-3	0.1	0.995
α	1e-4	1e-3	0.1	0.99
ϵ_{HOMO}	1e-3	0	0.01	0.95
ϵ_{LUMO}	5e-4	1e-6	0.01	0.9
$\Delta\epsilon$	1e-3	0	0.01	0.99
$\langle R^2 \rangle$	5e-4	1e-4	0.1	0.99
ZPVE	5e-4	1e-5	0.001	0.99
U_0	1e-4	1e-4	0.01	0.99
U	1e-4	0	0.01	0.9
H	1e-4	1e-4	0.01	0.9
G	1e-4	1e-5	0.01	0.995
C_v	1e-4	1e-5	0.01	0.995

787
788
789
790 B.2 GNN+ DATASETS
791

792
793 We keep the hyperparameters for the different datasets and models the same as in the original paper,
794 except for the number of epochs, weight decay, and learning rate. As we are training with 10% of the
795 original data, we double the number of epochs to mitigate the fewer parameter updates. We then made
796 a two-step hyper-parameter sweep; initially the learning rate using original weight decay values, and
797 afterwards the weight decay using the found best learning rates. The learning rates investigated were
798 (0.25, 0.5, 1.0, 2.0, 4.0) times the original learning rate value for that model and dataset. The weight
799 decays investigated was $(10^{-6}, 10^{-5}, 10^{-4}, 10^{-3}, 10^{-2}, 10^{-1}, 0)$. We could not simply multiply the
800 weight decay values by a fixed factor, as some of the original weight decay values were 0. These
801 sweeps were performed for a single uncoupled model following the same tuning procedure as in
802 the original paper. Notably, this means that the predictive accuracy report from each run is the best
803 validation performance seen during any of the epochs. The found learning rates are listed in Table 13,
804 and weight decays Table 13 below. The train, validation, and test splits follow the same procedure as
805 Luo et al. (2025). Each seed shuffles the labeled and unlabeled part of the training data.

806
807 The SSL parameters were selected based on the best performing values on the validation score on
808 ZINC. The mean-teacher values investigated was $(0.9, 0.99, 0.995, 0.999)$, and the coupling weight
809 for the consensus and pair-wise methods were $(0.25, 0.5, 0.75, 1, 1.25, 1.5, 1.75, 2.0)$. The optimal
810 value of mean-teacher was found to be 0.999, and coupling weight for the consensus learning
811 was 1.0, and the pairwise loss was tied between 0.5 and 0.75, so we went with 0.5 based on the
812 recommendations in Filipiak et al. (2022).

810
811 Table 12: Tuned learning rates for GNN models across datasets.
812
813
814
815
816
817
818
819
820
821
822
823
824

Dataset	GCN	GINE	GATEDGCN
CIFAR-10	0.002	0.0005	0.001
CLUSTER	0.0005	0.0005	0.002
ogbg-molhiv	0.0001	0.00005	0.0004
MalNet-Tiny	0.00025	0.002	0.002
MNIST	0.001	0.002	0.001
PATTERN	0.004	0.001	0.000125
ogbg-molpcba	0.000125	0.000125	0.00025
peptides-func	0.0005	0.002	0.002
peptides-struct	0.002	0.0005	0.002
ogbg-ppa	0.0006	0.0012	0.0003
PascalVOC-SP	0.004	0.002	0.0005
ZINC	0.004	0.001	0.004

825
826
827
828
829
830
831
832
833
834
835
836
837
838 Table 13: Tuned weight decays for GNN models across datasets.
839
840

Dataset	GCN	GINE	GATEDGCN
CIFAR-10	10^{-2}	10^{-1}	10^{-2}
CLUSTER	0	10^{-1}	10^{-6}
ogbg-molhiv	10^{-3}	10^{-1}	10^{-5}
MalNet-Tiny	10^{-4}	10^{-2}	10^{-4}
MNIST	10^{-1}	10^{-2}	10^{-5}
PATTERN	10^{-3}	10^{-2}	10^{-1}
ogbg-molpcba	10^{-1}	10^{-2}	10^{-5}
peptides-func	0	10^{-1}	10^{-3}
peptides-struct	10^{-3}	10^{-5}	10^{-1}
ogbg-ppa	10^{-1}	10^{-1}	10^{-2}
PascalVOC-SP	10^{-1}	10^{-4}	10^{-2}
ZINC	10^{-1}	10^{-5}	10^{-3}

853
854
855
856
857
858
859 B.3 CIFAR-10
860
861
862
863

The hyperparameter configurations for CIFAR-10 are shown in Table 14.

864
865 Table 14: Hyperparameter Configuration for CIFAR-10.
866
867
868
869
870
871
872
873
874
875
876
877
878
879
880
881
882
883
884

Hyperparameter	Value
Learning Rate	
Learning rate	0.005
Annealing method	Step
Step size	1
Learning rate reduction	0.975
Regularization	
L2 Weight Decay	0.075
Optimizer	
Optimizer	SGD
Momentum	0.9
Training	
Epochs	250
Loss Function	
Coupled loss weighting	1.0
Ensemble coupled loss	KL-divergence
Supervised loss	Cross-entropy

885
886
887

C CALIBRATION SCORES FOR THE OGBG-MOLHIV

888
889

890 We also investigate the calibration on the ogbg-molhiv benchmark. We do not investigate the datasets
891 ogbg-pcba and peptides functional due to the to the large skewing of classes and missing values. The
892 results are included in Table 15 and Table 16. We see across different architectures that the coupling
893 of the ensemble improves the calibration scores, especially NLL. One notable exception is the MCE
894 score for the GIN ensemble model, where the coupled ensemble becomes significantly worse.

895
896897 Table 15: Individual Performance on the ogbg-molhiv dataset
898

Metric	GCN		GIN		GatedGCN	
	Decoupled	Coupled	Decoupled	Coupled	Decoupled	Coupled
Accuracy	95.78 \pm 0.38	96.18 \pm 0.48	95.97 \pm 0.68	96.30 \pm 0.35	95.66 \pm 0.72	96.01 \pm 0.57
ROC-AUC	.721 \pm .0193	.731 \pm .0218	.733 \pm .017	.734 \pm .015	.731 \pm .008	.736 \pm .007
NLL	.375 \pm .185	.230 \pm .0662	.147 \pm .015	.140 \pm .012	.200 \pm .033	.180 \pm .023
ECE	.0312 \pm .0092	.0246 \pm .0039	.0113 \pm .0045	.0105 \pm .0048	.0232 \pm .0069	.0201 \pm .0049
MCE	.2041 \pm .0994	.2058 \pm .0763	.1113 \pm .0620	.1058 \pm .0246	.1154 \pm .0399	.0985 \pm .0287

905
906
907
908 Table 16: Ensemble Performance on the ogbg-molhiv dataset
909

Metric	GCN		GIN		GatedGCN	
	Decoupled	Coupled	Decoupled	Coupled	Decoupled	Coupled
Accuracy	96.66 \pm 0.33	96.60 \pm 0.20	96.11 \pm 0.66	96.39 \pm 0.33	96.03 \pm 0.62	96.12 \pm 0.56
ROC-AUC	.7350 \pm .0228	.7357 \pm .0212	.7346 \pm .0165	.7347 \pm .0153	.7341 \pm .0107	.7383 \pm .0073
NLL	.2437 \pm .1051	.1760 \pm .0275	.1432 \pm .0130	.1383 \pm .0108	.1821 \pm .0249	.1729 \pm .0208
ECE	.0261 \pm .0057	.0224 \pm .0046	.0121 \pm .0039	.0109 \pm .0037	.0201 \pm .0051	.0193 \pm .0045
MCE	.2587 \pm .0793	.2617 \pm .0564	.1585 \pm .0760	.1933 \pm .0852	.1566 \pm .0576	.1533 \pm .0251

918

D ABLATION STUDIES

919

920

D.1 SOFT OR HARD LABELS FOR CLASSIFICATION

921

922 Often semi-supervised methods use some form of "hard-labeling" as the consistency target. Usually,
923 this is implemented as setting the ensemble target for an unlabeled datapoint to be the most likely
924 label, as predicted by the individual model (Filipiak et al., 2022; Tarvainen & Valpola, 2018) or the
925 ensemble (Platanios, 2018). This removes the underlying uncertainty information of the estimates, and
926 risking drastically reducing the calibration of the model by making it overconfident. The motivation
927 for using hard-labeling is the assumption of label smoothness, as it forces the model to pick the
928 same label for data points close together. We investigate this assumption in table 17. The results
929 on accuracy show that hard-labelling slightly benefits the accuracy, it comes at the cost of worse
930 calibration metrics such as ECE and MCE for the individual models. The reason for such a small
931 increase in accuracy can be explained by the label-smoothening assumption can be violated for graphs
932 and especially molecules.

933

Table 17: Calibration metrics on graph CIFAR-10.

934

Metric	Non-Ensemble		Ensemble	
	Mean	Hard Label	Mean	Hard Label
Accuracy (%) \uparrow	56.0220 \pm 0.2233	56.2020 \pm 0.5595	56.7640 \pm 0.2742	57.1920 \pm 0.4124
ROC \uparrow	.9040 \pm .0017	.8936 \pm .0025	.7598 \pm .0015	.7621 \pm .0022
F1 \uparrow	.5586 \pm .0021	.5607 \pm .0051	.5661 \pm .0023	.5706 \pm .0034
ECE \downarrow	.1514 \pm .0030	.3034 \pm .0052	.4324 \pm .0027	.4281 \pm .0041
MCE \downarrow	.2307 \pm .0030	.4252 \pm .0141	.4324 \pm .0027	.4281 \pm .0041

944

D.2 PAIRWISE OR COUPLED ENSEMBLE

945

946 There is a strong theoretical connection between the pairwise loss between ensemble members used
947 in n-CPS and the coupled ensemble loss presented in this work. For a convex loss \mathcal{L} that can be
948 written on the form $\mathcal{L}(x - y)$, then Jensen's inequality yields

949
$$\begin{aligned} 950 \mathcal{L}(f_{\theta_i}(x) - \mathbb{E}_m[f_{\theta_m}(x)]) &= \mathcal{L}(\mathbb{E}_m[f_{\theta_i}(x) - f_{\theta_m}(x)]) \\ 951 &\leq \mathbb{E}_m[\mathcal{L}(f_{\theta_i}(x) - f_{\theta_m}(x))] \\ 952 &= \frac{1}{M} \sum_{m=1}^M \mathcal{L}(f_{\theta_i}(x) - f_{\theta_m}(x)) \\ 953 &\leq \frac{1}{M-1} \sum_{m=1}^M \mathcal{L}(f_{\theta_i}(x) - f_{\theta_m}(x)). \\ 954 \end{aligned}$$

955 As $f_{\theta_i}(x) - f_{\theta_m}(x) = 0$ if $i = m$ this upper bound is exactly the n-CPS loss. In general this upper
956 bound is not tight, but if $M = 2$ and \mathcal{L} is of the form $(x - y)^l$, e.g. the l_1 or l_2 -loss we get

957
$$\begin{aligned} 958 \mathcal{L}(f_{\theta_1} - \mathbb{E}_m[f_{\theta_2}(x)]) &= \left(f_{\theta_1} - \frac{f_{\theta_1} + f_{\theta_2}}{2} \right)^l \\ 959 &= \frac{1}{2^l} (f_{\theta_1} - f_{\theta_2})^l. \\ 960 \end{aligned}$$

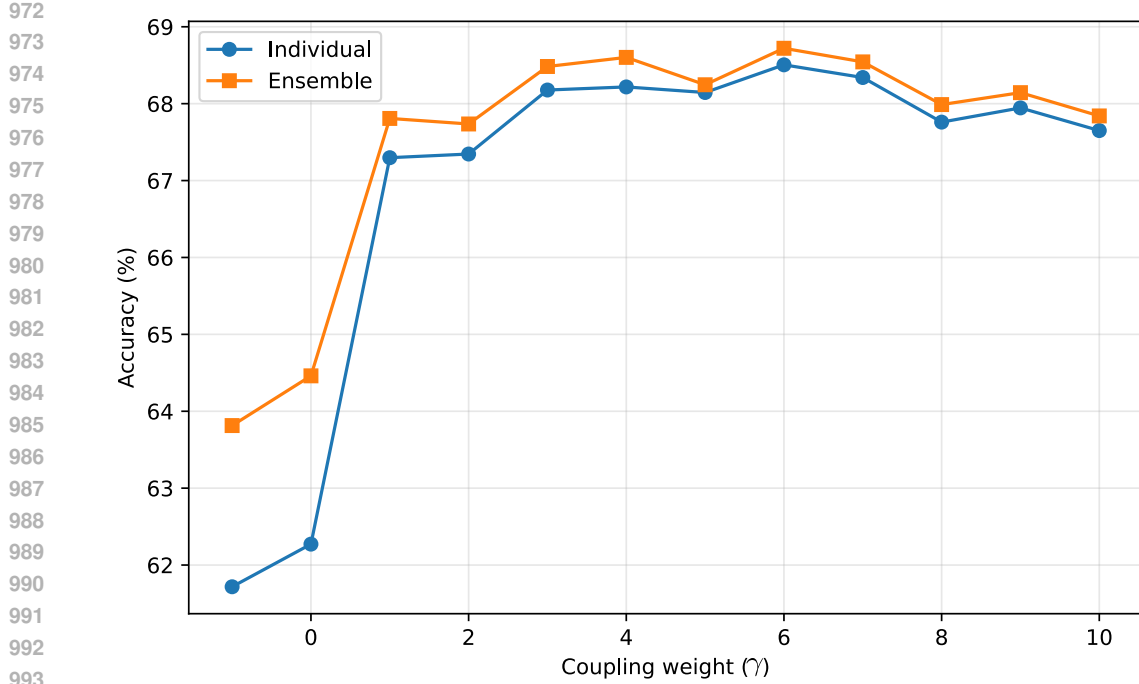
961 We see that the two losses are equal up to a scaling factor that disappears if we tune the learning rate.

962

D.3 ROBUSTNESS OF COUPLED WEIGHTING

963

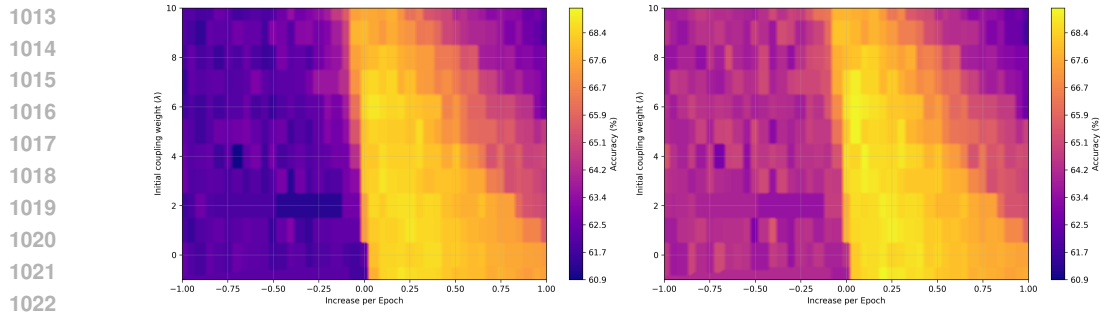
964 To investigate the robustness of the coupled weighting γ , we followed the same experimental setup
965 on CIFAR-10 with a Resnet18 model. The results can be seen in Figure 1. From the figure, we see
966 that the validation accuracy is somewhat flat as soon as $\gamma > 1$, but there is a small optimum around
967 $\gamma = 6$. This illustrates that at least for CIFAR-10, the choice of γ is robust.



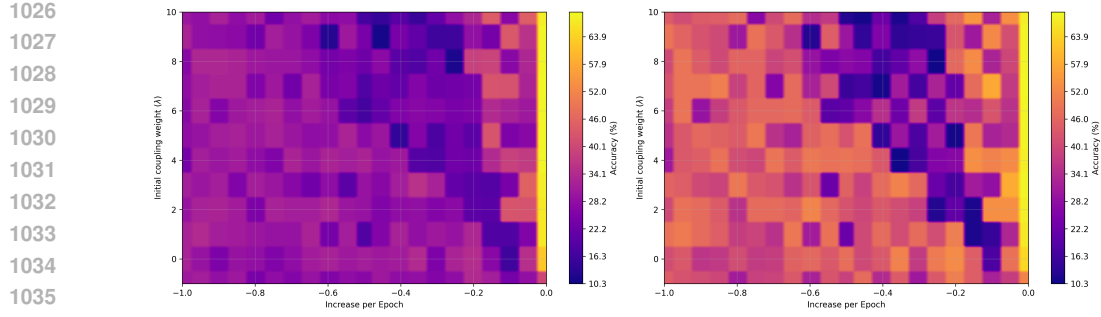
972
973
974
975
976
977
978
979
980
981
982
983
984
985
986
987
988
989
990
991
992
993
994
995
996 Figure 1: Validation accuracy as a function of the weighting of the ensemble consistency loss.
997
998
999
1000

D.4 HOW TO SCHEDULE THE COUPLED LOSS

1001 Initially, during training, the members of the ensemble models only have weak prediction strength.
1002 This results in the ensemble prediction serving only as a weak signal guiding the models. Intuitively,
1003 this suggests that the weighting of the coupled loss should be added or increased as training progresses.
1004 We investigate if this is the case in the same CIFAR-10 setting. We let the ensemble coupling
1005 weighting be a linear function of the number of epochs, and vary the starting value and slope of the
1006 ensemble coupling weighting. The results can be seen in Figure 2, where negative coupling weights
1007 are clipped to 0, while Figure 3 shows the un-clipped results (in the relevant area). From Figure 2, we
1008 see that for CIFAR-10, there is no large benefit to begin coupling later compared to selecting a good
1009 constant coupling value. Note that a delayed start corresponds to a negative start value and a positive
1010 increase pr. epoch, as an initial coupling of -1 and a pr. epoch increase of 0.1 means it starts at epoch
1011 10, due to clipping.
1012



1013
1014
1015
1016
1017
1018
1019
1020
1021
1022
1023
1024 Figure 2: Validation accuracy as a function of the initial coupling weight and the increase in coupling
1025 weights per epoch for an individual model (left) and a coupled ensemble with two members (right).
The results are averaged over 3 seeds.
1026



1026
1027
1028
1029
1030
1031
1032
1033
1034
1035
1036
1037
1038
1039
1040
1041
1042
1043
1044
1045
1046
1047
1048
1049
1050
1051
1052
1053
1054
1055
1056
1057
1058
1059
1060
1061
1062
1063
1064
1065
1066
1067
1068
1069
1070
1071
1072
1073
1074
1075
1076
1077
1078
1079
Figure 3: Validation accuracy as a function of the weighting of the ensemble consistency loss.

D.5 DIFFERENT LOSSES

We also investigated the sensitivity to different formulations of the ensemble consistency loss. The results are shown in Table 18. We ran with the same setup for the computer vision CIFAR-10 and two ensemble members. While the best performing loss function was KL-divergence (the same form as the supervised loss), the "regression" functions (L_1 , L_2 , L_∞) performed about the same. Only the reversed KL-divergence, $D_{KL}(E||I)$, resulted in lower accuracy, at around the same level as a decoupled model (see Table 4).

Table 18: Validation accuracy with different ensemble consistency loss functions. Results averaged over 10 seeds. Here, I is the individual prediction and E is the ensemble consensus.

Ensemble Loss	Individual Accuracy
L_∞	66.23 ± 0.29
$D_{KL}(I E)$	66.62 ± 0.51
$D_{KL}(E I)$	59.37 ± 0.78
L_1	66.01 ± 0.51
L_2	66.12 ± 0.45

D.6 DIFFERENT COUPLING STRATEGIES

We investigated different strategies for coupling the unsupervised loss on QM9. This includes various combinations of three parameters: the *coupling weight*, the *coupling start* and the *coupling schedule*.

Coupling weight The coupling weight parameter defines how much the unsupervised loss should contribute to the total loss. When set to 0, only the supervised loss will be taken into account.

Coupling start The coupling start refers to when the unsupervised loss is included during training, i.e. for the first $x\%$ of epochs, the model is only trained on the labeled data and only afterwards, the unsupervised loss will be included via coupling. Depending on the dataset and task, it intuitively can make sense to first let the model learn a little bit before evaluating the loss on unlabeled data. Specifically, in regression tasks this can be the case, since the model output is not bounded, as opposed to classification tasks. When set to 0, coupling will be used through the whole training. This parameter is given in percentage, i.e. percentage of total training epochs after which the coupling should start.

Coupling schedule Three different coupling schedules were tested: *constant*, *increase* and *bell*. *Constant* refers to the coupling weight being constant from onset until the end of training. *Increase* means that there will be a smooth ramp up until the coupling weight reaches its maximum (i.e. the coupling weight parameter). *Bell* means that there is a smooth bell curve over the coupling weight, i.e. first it increases, then decreases. Here, it will start and end at 0, and peak at a maximum which is set via the coupling weight parameter.

1080
1081
1082
1083
1084
1085
1086
1087
1088
1089
1090
1091
1092
1093
1094
1095
1096
1097
1098
1099
1100
1101
1102
1103
1104
1105
1106
1107
1108
1109
1110
1111
1112
1113
1114
1115
1116
1117
1118
1119
1120
1121
1122
1123
1124
1125
1126
1127
1128
1129
1130
1131
1132
1133

Figure 4 and Figure 5 shows the impact of different coupling strategies on the model performance, here for target 4 and 7 of QM9 respectively. We can see that a good choice of the coupling weight is crucial for our method to result in a significant improvement in MAE compared to the fully supervised baseline. The optimal coupling weight seems to differ per task, as both targets have a different optimum (0.1 for target 4 and 0.01 for target 7). A good value for the coupling start seems to depend on the choice of coupling weight, however a trend can be observed that for the best coupling weight options for each target, the optimal coupling start is 0, i.e. using coupling from the start of training. The optimal choice of coupling schedule seems to depend on both of the other choices, but in the specific case of target 4, the *increase* schedule led to the best performance. For target 7, the *bell* schedule resulted in the best ensemble performance, while the *constant* schedule led to the best individual performance.

One interesting finding here is that if we couple too strongly, meaning we are weighing the unsupervised loss to high, the ensemble performance gets worse than the baseline, while at the same time the individual members from the ensemble are outperforming the baseline. This is due to the models collapsing, so while each individual model is better than an individual model that was not coupled, ensembling has no significant benefit anymore.

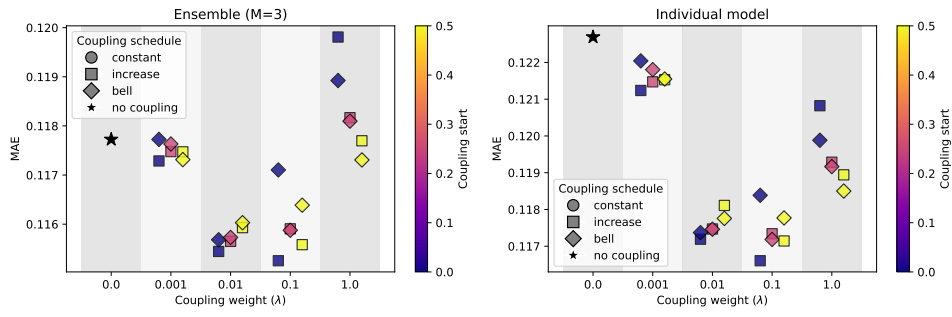


Figure 4: Performance (MAE) of coupled ensembles (left) and individual models from coupled ensembles (right) for different coupling strategies, for QM9 target 4.

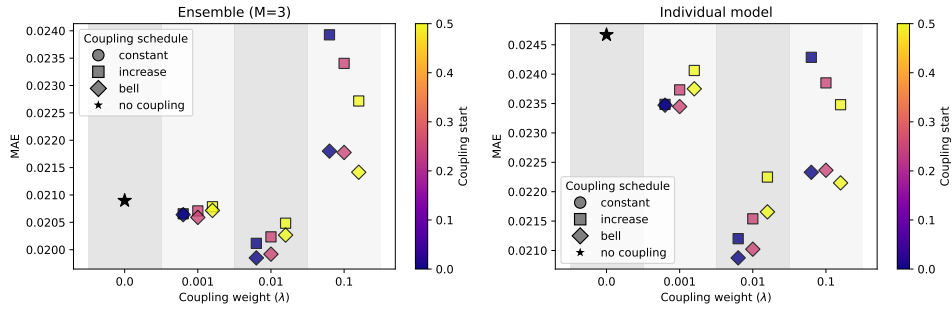


Figure 5: Performance (MAE) of coupled ensembles (left) and individual models from coupled ensembles (right) for different coupling strategies, for QM9 target 7.

D.7 EVALUATING OVERFITTING ON UNLABELED DATA

To evaluate potential overfitting to the unlabeled data, we compare the final model’s performance on the unlabeled training set against its performance on the unseen test set. For this analysis, we leverage our access to the ground-truth labels of the unlabeled set to compute its MAE. As presented in Table 19, the performance is nearly identical across both datasets for all 12 QM9 targets. This strong correspondence indicates that our method avoids overfitting to the unlabeled data used during training. This has a significant practical benefit, as it means the model’s predictions on the entire unlabeled set can be reliably used for downstream tasks.

1134
1135
1136
1137
1138
1139
1140
1141
1142
1143
1144
1145

1146 Table 19: PaiNN performance (MAE) on QM9 targets, comparing the held-out test set with the
1147 unlabeled dataset used during training. Results are reported for 3 seeds.

Target	Unit	Data	Individual Member	Ensemble (M=4)
μ	D	Test	.0619 \pm .0004	.0613 \pm .0004
		Unlabeled	.0597 \pm .0005	.0596 \pm .0005
α	a_0^3	Test	.1327 \pm .0002	.1307 \pm .0002
		Unlabeled	.1271 \pm .0003	.1264 \pm .0003
ϵ_{HOMO}	meV	Test	74.3067 \pm .2874	73.4216 \pm .2602
		Unlabeled	71.9862 \pm .3985	71.9587 \pm .3975
ϵ_{LUMO}	meV	Test	57.7005 \pm .3890	57.2248 \pm .3748
		Unlabeled	56.8535 \pm .2745	56.8405 \pm .2741
$\Delta\epsilon$	meV	Test	116.8389 \pm .7476	115.5238 \pm .7658
		Unlabeled	114.0289 \pm .4605	113.9998 \pm .4630
$\langle R^2 \rangle$	a_0^2	Test	.6189 \pm .0321	.5696 \pm .0320
		Unlabeled	.6011 \pm .0306	.5643 \pm .0303
ZPVE	meV	Test	2.0117 \pm .0072	1.9884 \pm .0077
		Unlabeled	1.9892 \pm .0065	1.9849 \pm .0065
U_0	meV	Test	19.9535 \pm .1812	19.3611 \pm .1819
		Unlabeled	19.2928 \pm .2250	18.9534 \pm .2191
U	meV	Test	20.1439 \pm .1736	19.5466 \pm .1586
		Unlabeled	19.5014 \pm .1851	19.1608 \pm .1790
H	meV	Test	20.1217 \pm .1890	19.5235 \pm .1905
		Unlabeled	19.4933 \pm .2367	19.1509 \pm .2335
G	meV	Test	20.2668 \pm .2044	19.6880 \pm .1955
		Unlabeled	19.7077 \pm .2041	19.3852 \pm .2030
C_v	$\frac{\text{cal}}{\text{mol K}}$	Test	.0450 \pm .0003	.0440 \pm .0004
		Unlabeled	.0443 \pm .0002	.0439 \pm .0002

1177
1178
1179
1180
1181
1182
1183
1184
1185
1186
1187